ISSN 1674-1056
http://cpb.iphy.ac.cn
http://iopscience.iop.org/cpb
中国物理 B
Chinese Physics
中国物理 Chinese Physics B

Synthesis of Pr-doped ZnO nanoparticles and their structure and optical and photocatalytic properties

Jun-Lian Chen(陈军联), Neena Devi, Na Li(李娜), De-Jun Fu(付德君), Xian-Wen Ke(柯贤文)

Citation: Chin. Phys. B . 2018, 27(8): 086102. **doi:** 10.1088/1674-1056/27/8/086102

Journal homepage: http://cpb.iphy.ac.cn; http://iopscience.iop.org/cpb

What follows is a list of articles you may be interested in

Influence of nitrogen and magnesium doping on the properties of ZnO films

Dong-hua Li(李东华), Hui-Qiong Wang(王惠琼), Hua Zhou(周华), Ya-Ping Li(李亚平), Zheng Huang(黄政), Jin-Cheng Zheng(郑金成), Jia-Ou Wang(王嘉鸥), Hai-jie Qian(钱海杰), Kurash Ibrahim(奎热西), Xiaohang Chen(陈晓航), Huahan Zhan(詹华瀚), Yinghui Zhou(周颖慧), Junyong Kang(康俊勇)

Chin. Phys. B . 2016, 25(7): 076105. **doi:** 10.1088/1674-1056/25/7/076105

Effects of N doping on photoelectric properties of along different directions of ZnO bulk and nanotube

Zheng Hong-Mei, Fang Xiao-Yong, Cai Li-Xia, Yin Ai-Cha, Jin Hai-Bo, Yu Xiao-Xia, Cao Mao-Sheng

Chin. Phys. B . 2014, 23(12): 126102. **doi:** 10.1088/1674-1056/23/12/126102

Improving light trapping and conversion efficiency of amorphous silicon solar cell by modified and randomly distributed ZnO nanorods

Jia Zhi-Nan, Zhang Xiao-Dan, Liu Yang, Wang Yan-Feng, Fan Jun, Liu Cai-Chi, Zhao Ying

Chin. Phys. B . 2014, 23(4): 046106. **doi:** 10.1088/1674-1056/23/4/046106

Optical study of D–D neutron irradiation-induced defects in Co- and Cu-doped ZnO wafers

Wang Yun-Bo, Li Gong-Ping, Xu Nan-Nan, Pan Xiao-Dong

Chin. Phys. B . 2013, 22(3): 036102. **doi:** 10.1088/1674-1056/22/3/036102

Detection of Fe 3d electronic states in valence band and magnetic properties of Fe-doped ZnO film

Chen Tie-Xin, Cao Liang, Zhang Wang, Han Yu-Yan, Zheng Zhi-Yuan, Xu Fa-Qiang, Ibrahim Kurash, Qian Hai-Jie, Wang Jia-Ou

Chin. Phys. B . 2013, 22(2): 026101. **doi:** 10.1088/1674-1056/22/2/026101

Synthesis of Pr-doped ZnO nanoparticles: Their structural, optical, and photocatalytic properties*

Jun-Lian Chen(陈军联)[1,2], Neena Devi[2], Na Li(李娜)[1,2], De-Jun Fu(付德君)[2,†], and Xian-Wen Ke(柯贤文)[1]

[1] School of Printing and Packaging, Wuhan University, Wuhan 430072, China

[2] Hubei Key Laboratory of Nuclear Solid Physics and School of Physics and Technology, Wuhan University, Wuhan 430072, China

(Received 11 April 2018; revised manuscript received 8 May 2018; published online 10 July 2018)

Undoped and praseodymium-doped zinc oxide (Pr-doped ZnO) (with 2.0-mol%–6.0-mol% Pr) nanoparticles as sunlight-driven photocatalysts are synthesized by means of co-precipitation with nitrates followed by thermal annealing. The structure, morphology, and chemical bonding of the photocatalysts are studied by x-ray diffraction (XRD), scanning electron microscopy (SEM) with energy dispersive x-ray emission spectroscopy (EDS), x-ray photoelectron spectroscopy (XPS), and Fourier transform infrared spectroscopy (FTIR), respectively. The optical properties are studied by photoluminescence (PL) and UV-vis diffuse reflectance spectroscopy (UV-vis DRS). We find that Pr doping does not change the crystallinity of ZnO; but it reduces the bandgap slightly, and restrains the recombination of the photogenerated electron–hole pairs. The photocatalytic performance of the photocatalysts is investigated by the photodegradation reaction of 10-mg/L rhodamine B (RhB) solution under simulated sunlight irradiation, showing a degradation rate of 93.75% in ZnO doped with 6.0-mol% Pr.

Keywords: ZnO, Pr-doped, photocatalytic activity

PACS: 61.72.uj, 82.45.Jn, 82.45.–h **DOI:** 10.1088/1674-1056/27/8/086102

1. Introduction

Pesticides, dyes, and heavy metals in water may cause environmental pollution.[1] Among these pollution sources, organic dyes are widely used in the leather, textile, pulp, cosmetic, and pharmaceutical industries and they are dominating pollutants in waste water. These dyes are toxic and carcinogenic, so they may affect the health of living things on Earth.[2–4] However, these stubborn organic pollutants are carbon-based chemical substances which are not easy to degrade naturally and may not be entirely eliminated by the conventional techniques or manner like biological, physical, and chemical processes. It can be of high operational cost to adopt the expensive chemicals and electricity consumption in order to remove the pollutants completely, owing to their stability to the oxidants, which consumes huge energy resources and produces perilous secondary pollutants, such as toxic sludge, heavy metals, and solid waste.[4–6]

Facing the problems of environmental pollution and exhaustion of energy sources, the search for new energy has attracted extensive attention of researchers. It has been proved that multi-phase semiconductors have great potential for the following applications in the new energy sector: photocatalytic and electrocatalytic production of hydrogen from water[7–10] and photocatalytic elimination of toxic chemicals in water.[11] Among the numerous semiconductors used in the field of photocatalysis such as ZnO,[12] ZnS,[13] TiO_2,[14] and Fe_2O_4,[15] ZnO is one of the most common materials due to its stable chemical nature, low cost, and non-toxic characters.[16] It is widely used in solar cells, sensors, catalysts, luminescence, optoelectronics, biomedical devices, and light-emitting diodes.[17–20] However, its wide bandgap (3.37 eV) means that it can absorb only UV light ($\lambda < 368.0$ nm) that occupies only 3%–5% of the sunlight; this restricts the utilization of the complete solar energy spectrum and leads to low quantum efficiency.[21,22] Besides, the separation of photogenerated electrons from vacancies needs to be strengthened for enhancing the photo-quantum efficiency.[6] Therefore, making the ZnO photocatalyst respond to the solar spectrum and promoting the separation of photogenerated electron–hole pairs have become one of the biggest challenges.[23]

Researches in recent years have indicated that the performance of semiconductor photocatalysts can be enhanced through modification with metal and/or nonmetal doping, and the spectral response is also improved, with the better utilization of the sunlight.[24] Therefore, modified photocatalysis based on semiconductor oxides proves to be a good technology for treating the environmental pollution, and has become a rather popular research topic over the past few years.[25]

Rare earth doped materials applied to optical light-emitting phosphors and other optoelectronics devices have aroused broad interest.[26] Furthermore, rare earth materials are important for photocatalytic techniques because of the dif-

*Project supported by the International Cooperation Program of the Ministry of Science and Technology of China (Grant No. 2015DFR00720), the Cooperation Program of Wuhan Science and Technology Bureau, China (Grant No. 2016030409020219), and the Shenzhen Committee on Science and Technology Innovation, China (Grant No. JCYJ20170818112901473).

†Corresponding author. E-mail: djfu@whu.edu.cn

© 2018 Chinese Physical Society and IOP Publishing Ltd

ferent special interband 4f–5d and intraband 4f–4f electronic transitions compared with other element groups. Hence, combining rare earth elements with a ZnO matrix may enable pollutants to be absorbed onto the photocatalyst surface.[27] There are 17 elements in lanthanide elements, but researches on rare earth-doped ZnO photocatalysts are still rather deficient. Matarangolo *et al.* reported that a Pr-doped ZnO photocatalyst showed the better photocatalytic performance for discolorating and mineralizing Eriochrome Black T in aqueous solution both under UV and visible-light illumination than Ce- or Eu-doped ZnO photocatalysts.[5] However, the photodegradation of the RhB dye in water by the Pr-doped ZnO photocatalyst under the solar light illumination has not been reported. For this reason, we intend to study the effects of Pr-dopant on the structural, morphologic, and optical properties of ZnO nanoparticles and to investigate the photocatalytic activity depending on Pr-dopant concentration tested in removal of RhB dye in aqueous solution under simulated sunlight irradiation.

In the present paper, Pr-doped ZnO samples are synthesized through co-precipitating by using zinc nitrate hexahydrate ($Zn(NO_3)_2{\cdot}6H_2O$), praseodymium nitrate hexahydrate ($PrN_3O_9{\cdot}H_2O$), trisodium citrate dihydrate ($C_6H_5Na_3O_7{\cdot}2H_2O$), and sodium hydroxide (NaOH), the microstructure, morphology, and optical features of photocatalysts are characterized by x-ray diffraction (XRD), scanning electron microscopy (SEM) equipped with energy dispersive x-ray spectrometer (EDS), x-ray photoelectron spectroscopy (XPS), Fourier transform infrared spectroscopy (FTIR), photoluminescence (PL), and UV-vis diffuse reflectance spectra (UV-vis DRS). The Rhodamine B (RhB) removal efficiency under simulated sunlight illumination is investigated to evaluate the photocatalytic activity of the prepared ZnO:Pr nanoparticles.

2. Experimental section

2.1. Synthesis of Pr-doped ZnO photocatalysts

Zinc nitrate hexahydrate ($Zn(NO_3)_2{\cdot}6H_2O$), praseodymium nitrate hexahydrate ($PrN_3O_9{\cdot}H_2O$), trisodium citrate dihydrate ($C_6H_5Na_3O_7{\cdot}2H_2O$), and sodium hydroxide (NaOH) were used for the chemical synthesis. All these reactants were analytic reagents and no further purification was performed in the work. Deionized water was employed in all the synthesis processes.

A series of $Zn_{1-x}Pr_xO$ (with $x = 0$, 0.02, 0.04, 0.06) photocatalysts was synthesized by co-precipitating with nitrates. In a typical run, zinc nitrate hexahydrate and praseodymium nitrate hexahydrate were dissolved in 300-ml deionized water in a given value of substance ratio and agitated magnetically to obtain well-proportioned and stable solutions. After 15 min and 60 min, respectively, trisodium citrate dihydrate and sodium hydroxide were added to the solution. After 2 h, the magnetic mixer was turned off and the white precipitate was produced. Then, the precipitates were filtered separately and washed repeatedly with absolute ethyl alcohol to wipe off the unreacted chemicals. The product was then dried at 80 °C for 14 h. In this way, nanoparticle samples of ZnO, $Zn_{0.98}Pr_{0.02}O$, $Zn_{0.96}Pr_{0.04}O$, and $Zn_{0.94}Pr_{0.06}O$ were produced. Finally, these samples were heated at a temperature of 240 °C for 2 h.

2.2. Characterization of samples

The structural characterization of the synthetic photocatalysts was carried out with an x-ray diffractometer (D8 Advance, BRUKER) by using Cu Kα radiation ($\lambda = 0.1542$ nm). The 2θ range is 20°–80° and the scanning step is 0.02°. The morphologies of the samples were observed by SEM (SIRION, FEI) along with EDS. The chemical compositions of the samples as well as the valences of elements were investigated by XPS (Thermo Fisher ESCALAB 250 Xi) and all spectra were calibrated with the C 1s core level spectrum at a binding energy of 284.6 eV. The infrared spectra were recorded by Fourier transform infrared (FTIR) spectroscopy (FTIR5700, Thermo USA) in a wavenumber range of 500 cm^{-1}–4000 cm^{-1} to investigate the chemical bonds of the photocatalysts. The PL spectra were surveyed on a Raman spectrophotometer (RM1000, Renishaw) by using an Ar ion laser with an excitation wavelength of 325 nm. The UV-vis DRS spectra in a wavelength of 300 nm–600 nm were recorded through a UV-vis spectrophotometer (Lambda 35, PerkinElmer) with an integrating sphere for determining the bandgap of photocatalysts.

2.3. Photocatalysis experiments

The photocatalytic properties of the samples were investigated by the photodegradation for RhB dyes. In a typical run, 5 mg of photocatalysts were suspended in 10 ml of RhB solution with a concentration of 10 mg/L. Then, the suspension was gently stirred for 30 min in the dark to make the photocatalyst well dispersed and to reach adsorption–desorption balance. Next, the suspensions were irradiated by a mercury-tungsten combined light lamp (300 W, involving the UV and visible light region to simulate the solar conditions). A 2-ml suspension was sampled at 15-min intervals for centrifuging at a speed of 5000 rpm for 5 min. Then, the supernatant liquid of the solution was poured into a quartz glass, and the UV-vis absorption spectra ranging from 650 nm to 450 nm in wavelength were recorded by an S2500 spectrophotometer (UV-2550, SHMADZU) to monitor the process of photodegradation. The concentration of RhB was determined by the absorbance value of the solution located at 554 nm of the UV-vis spectrum.

3. Results and discussion

3.1. Structure and morphology

Figure 1(a) shows the XRD spectra in a range 20°–60° of the undoped ZnO and Pr-doped ZnO samples. The sharp and narrow peaks mean that the samples obtained are polycrystalline.[26] It can be seen that all the diffraction peaks of the crystallographic planes (100), (002), (101), (102), and (110) in the diffraction patterns are consistent with the data of the JCPDS No. 36-1451,[28] which indicates that samples have the hexagonal wurtzite structure and Pr doping does not cause evident change of the ZnO crystal structure. There is no additional peak in the diffraction spectrum, which means that no secondary impurity phases are found within the sensitivity of the technique. Also no characteristic peak of praseodymium oxide is found in the Pr-doped ZnO sample, which is believed to result from the low doping concentration and the location of dopants at Zn sites.

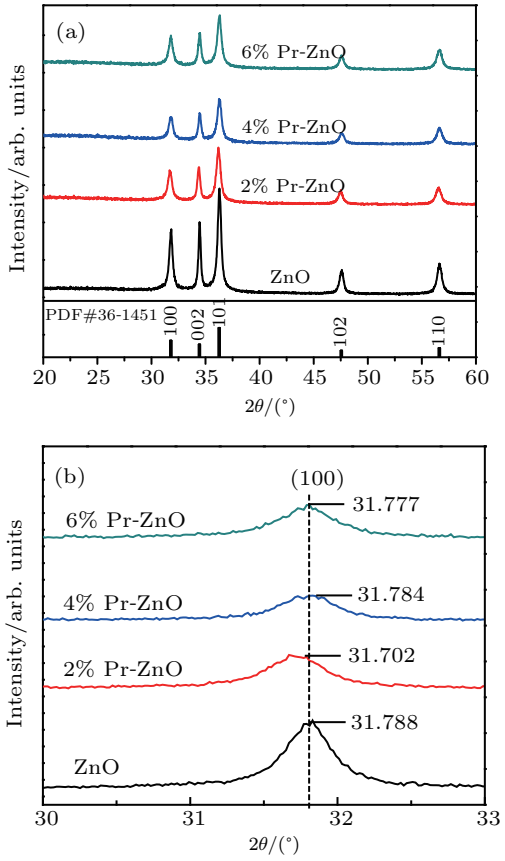


Fig. 1. (color online) (a) XRD spectra in a range 20°–60° of pure ZnO and Pr-doped ZnO nanoparticle samples. The bottom shows the values from standard JCPDS No. 36-1451 card of pure ZnO, (b) XRD spectra in a range 30°–33° of pure ZnO and Pr-doped ZnO nanoparticle samples.

It is worth noting that in a range of 30°–33° of the XRD spectrum (Fig. 2(b)), the peak position of the (100) plane has a small shift towards lower angles after doping. This slight shift of the diffraction peak results from the expansion of the ZnO lattice, which is caused by the difference in radius between praseodymium ion (1.01 Å) and zinc ion (0.74 Å). The variation of the ZnO lattice parameter is because of the substitution of praseodymium ions for zinc sites.[2,3]

The average crystallite sizes of the as-obtained nanoparticles were estimated by the peaks at a diffraction angle of 36° by using Debye–Scherrer's equation:

$$D = K\lambda/\beta\cos\theta, \tag{1}$$

where K is the Scherrer constant ($K = 0.89$), λ is the x-ray wavelength ($\lambda = 1.54$ Å), β is the diffraction angle of 36° (0.628 rad), and D is the corresponding full width at half maximum (FWHM) value of the diffraction peak. The crystallite sizes of undoped ZnO, 2.0-mol% Pr-doped ZnO, 4.0-mol% Pr-doped ZnO, and 6.0-mol% Pr-doped ZnO are 23.35 nm, 18.65 nm, 21.55 nm, and 18.57 nm, respectively. It is obvious that the crystallite size decreases after doping of Pr, which is because Pr^{3+} would hinder the diffusion and growth of ZnO crystallites, consistent with the fact that Pr^{3+} has a larger ionic radius than Zn^{2+} (see Ref. [2]).

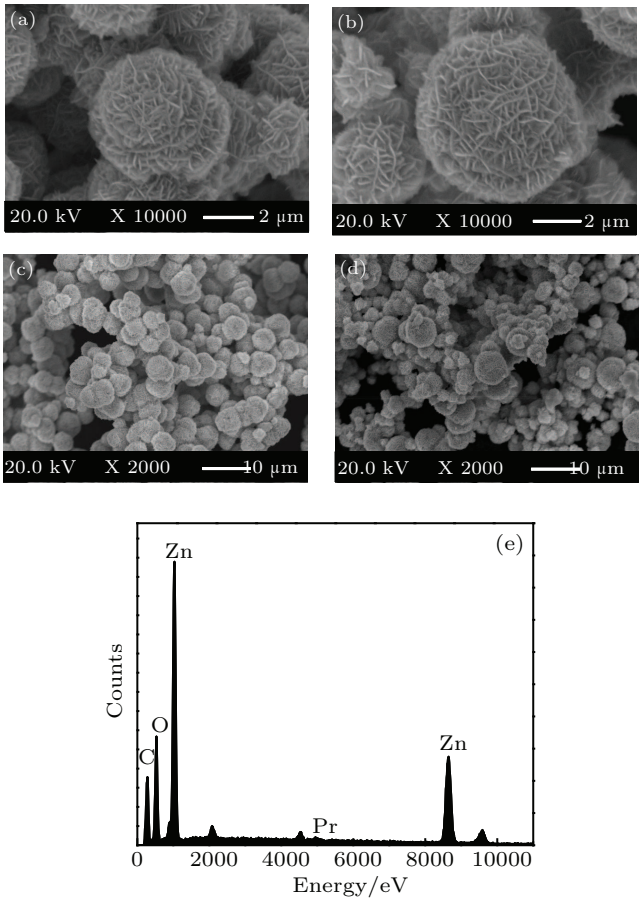


Fig. 2. SEM images of (a) undoped ZnO and (b) 2-mol% Pr-doped ZnO shown on a scale of 2 μm, (c) pure ZnO, and (d) 2-mol% Pr-doped ZnO shown on a scale of 10 μm, and (e) EDS spectrum of the 2.0-mol% Pr-doped ZnO sample.

Figures 2(a) and 2(b) show the SEM images of undoped ZnO and 2.0-mol% Pr-doped ZnO on the scale of 2 μm, while figures 2(c) and 2(d) show those two on a scale of 10 μm. The dopant of Pr does not significantly change the morphology of ZnO, and the 2-mol% Pr-doped ZnO sample is selected

as the representative of the doped samples. It can be seen that the samples consist of numerous macro aggregates. The agglomerated particles are mostly spherical and inhomogeneous in size, which is because of the aggregation of ZnO nanoparticles and the growth of irregular nanocrystals in the preparation process.[2] Figure 2(e) shows the EDS result, revealing that the samples are composed predominantly of Zn and O but with a trace amount of the Pr element.

3.2. Chemical bonding properties

The elemental composition and chemical bonds in Pr-doped ZnO samples are measured and the incorporation of Pr into ZnO lattice was confirmed by the XPS analysis. The XPS scan in a binding energy range of 0 eV–1300 eV of the 2.0-mol% Pr-doped ZnO shows that the photocatalyst consists mainly of Zn, O, and Pr element[27] (Fig. 3(a)). From the Zn 2p core level spectrum of the 2-mol% Pr-doped ZnO (Fig. 3(b)), the peak of Zn $2p_{3/2}$, and the peak of Zn $2p_{1/2}$ located, respectively, at 1020.8 eV and 1043.9 eV are in line with the standard binding energy of Zn and can be attributed to Zn–O bonds. The O 1s spectrum (Fig. 3(c)) is deconvolved with Gaussian Lorentzian mixed functions, giving two peaks. One is located at 530.93 eV in accordance with the Zn–O–Zn bond, and the other is positioned at 529.53 eV and attributed to the Pr–O–Pr bond consistent with the binding energy of Pr_2O_3, which again confirms the successful doping of Pr into the ZnO lattice. The Pr $3d_{3/2}$ and Pr $3d_{5/2}$ peaks located, respectively, at 953.7 eV and 932.8 eV (Fig. 3(d)) agree with the standard binding energy of Pr.

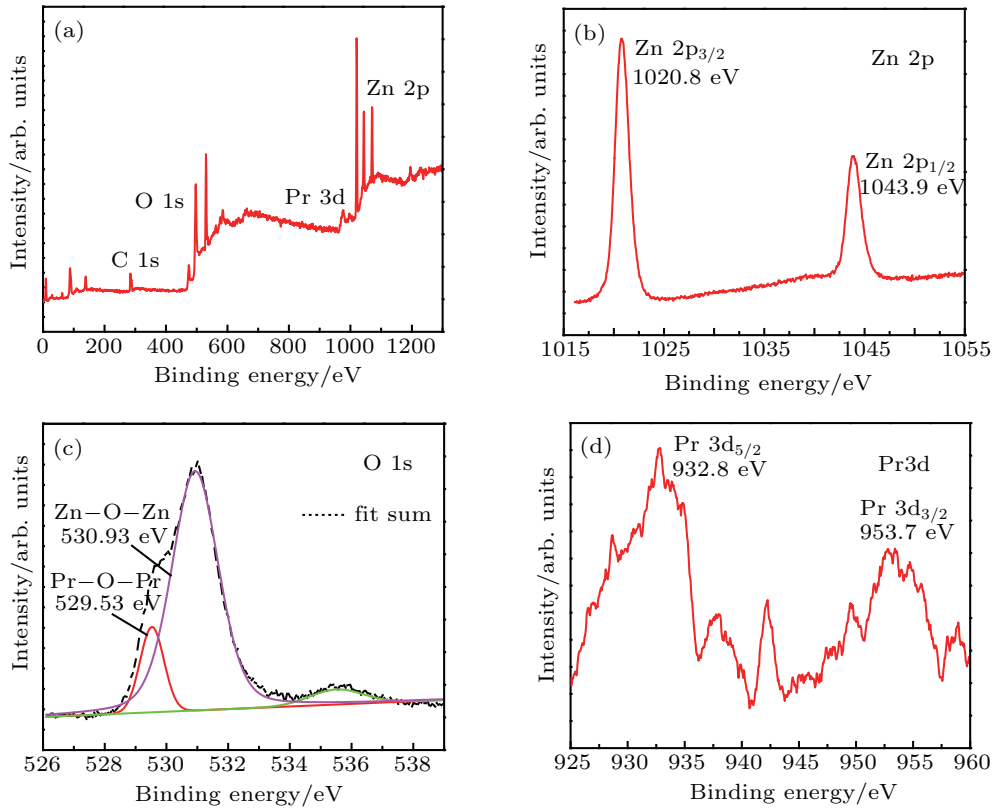


Fig. 3. (color online) (a) XPS survey of 2.0-mol% Pr-doped ZnO, core level spectra of (b) Zn 2p, (c) O 1s, and (d) Pr 3d.

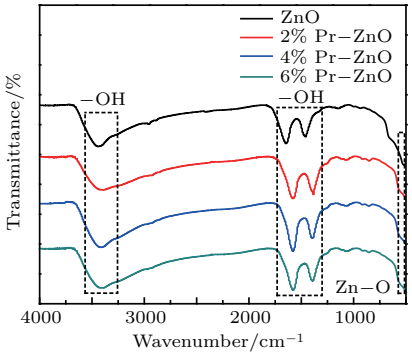


Fig. 4. (color online) FTIR spectra of pure and Pr-doped ZnO nanoparticle samples.

To identify the presence of functional groups, FTIR spectra of pure and Pr-doped ZnO photocatalysts are measured, and the results are shown in Fig. 4. The peak at 510 cm^{-1} results from ZnO vibration,[26] which is a characteristic absorption peak of ZnO. The broad peaks at 3418 cm^{-1}–3500 cm^{-1} and 1384 cm^{-1}–1600 cm^{-1} correspond to the stretching and bending vibrations of OH in the adsorbed water molecules, respectively, which proves the presence of Pr^{3+} indirectly because of its water absorption.[2] No evident impurity is found in the samples, as there are no further distinguished peaks associated with other functional groups.

3.3. Optical properties

To investigate the optical properties, room temperature photoluminescence is measured in the wavelength range of 350 nn–800 nm as shown in Fig. 5. The spectra each have a strong ultraviolet (UV) peak at 400 nm, along with a broad weak peak centered at 550 nm. The UV peak apparently originates from a recombination of free excitons.[29] The main feature is an evident decrease of the UV peak intensity with Pr doping, which indicates a decrease in the recombination rate of the photogenerated carriers, and this may result from the doped Pr^{3+} ions that act as traps to capture the photogenerated electrons or holes. The weak visible emissions are most likely associated with the singly ionized oxygen vacancies in the products, which result in the recombination of photogenerated holes with the electrons of the oxygen vacancies. It has been shown that more defects could be produced in the nanoparticle samples due to the incorporation of the dopants into the ZnO lattice,[30] for example, the substitution of praseodymium ions for zinc ones leads to the generation of oxygen defects for keeping electrical neutrality.[31] Hence, the doping of Pr into the ZnO lattice significantly weakens the band edge emission and increases the visible emission.[26] Finally, according to the wavelength of the ultraviolet emission peak, the bandgaps of the pure and 2.0-mol% Pr-doped ZnO are estimated at 3.12 eV while those of the 4.0-mol% and 6.0-mol% Pr-doped ZnO are calculated to be 3.11 eV. The bandgap is not significantly changed with the doping of Pr, because of the small doping level; but with an even larger amount of Pr dopant, such as 6.0 mol%, the bandgap reduction is still observable.

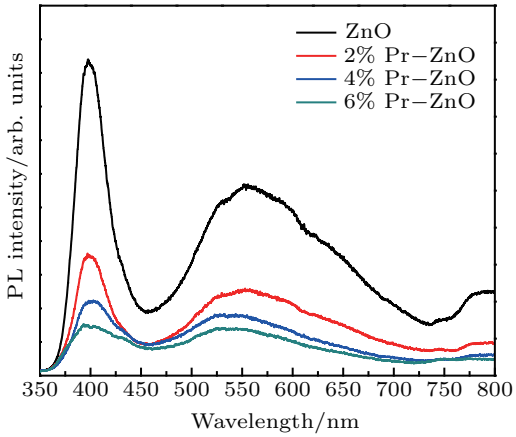


Fig. 5. (color online) PL spectra of the doped and undoped ZnO samples.

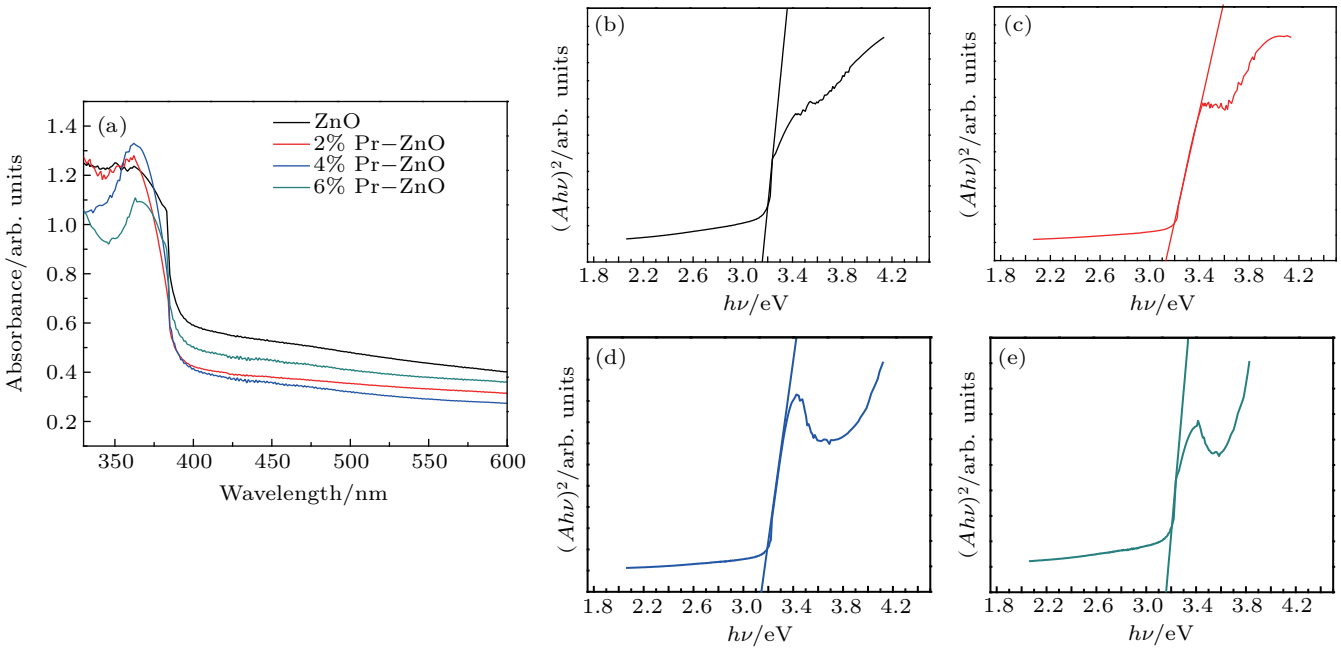


Fig. 6. (color online) (a) Absorption spectra of pure and Pr-doped ZnO samples, the Tauc plots given bandgaps of (b) pure, (c) 2-mol%, (d) 4-mol%, and (e) 6-mol% Pr-doped ZnO.

To investigate the optical absorption properties, the UV-vis DRS spectra in a range 300 nm–600 nm are measured as shown in Fig. 6(a). The optical bandgaps of the prepared photocatalysts are estimated using the Tauc equation (for direct bandgap semiconductor):

$$\left(\frac{h\nu}{K}\right)^2 = h\nu - E_g, \tag{2}$$

where A is the absorbance of UV-vis diffuse reflectance, E_g is the bandgap, and K is a constant. The value of E_g is not affected by the value of K. Through extrapolating the linear region of the plot $(Ah\nu)^2 \sim h\nu$, the optical bandgap of the samples can be estimated in a range of 3.11 eV–3.12 eV (Figs. 6(b)–6(e)). The bandgap for Pr-doped ZnO slightly decreases after the incorporation of moderate amounts of Pr dopant compared with for undoped ZnO. The slight decrease of bandgap may result from the impurity levels due to the sub-

stitutional Pr^{3+} in ZnO. It is easier for Pr-doped ZnO with narrower bandgaps than for undoped ZnO to generate more electron-hole pairs and hydroxyl radicals.[21]

3.4. Photodegradation of RhB

To study the photocatalytic properties of the synthesized samples with different Pr dopant concentrations, the photocatalytic degradation process of rhodamine B in aqueous solution under a simulated sunlight illumination is measured as shown in Figs. 7(a)–7(d). Figures 8(a)–8(b) show the photodegradation curves (C/C_0 versus time, where C and C_0 are the instantaneous and initial concentration of RhB, respectively) and degradation rates of rhodamine B by using various photocatalysts irradiated with simulated sunlight for 45 min. The degradation rate η of the RhB solution is calculated by using the following equation:

$$\eta = (C_0 - C_t)/C_0, \tag{3}$$

where C_t is the final concentration of RhB. It can be seen that the concentration of the RhB dye declines dramatically during the photodegradation process compared with that of the pure RhB solution. It is obvious that adding the dopant of Pr leads to enhanced photocatalytic activity, and the 6.0-mol% Pr-doped ZnO photocatalyst exhibits a high degradation efficiency, up to 93.75% degradation after 45-min irradiation. It is interesting that 2.0-mol% Pr-doped ZnO photocatalyst (69.12% degradation) does not exhibit better photocatalytic performance compared with undoped ZnO (79.87% degradation). The photocatalytic performance of photocatalyst can be influenced to an extent as big as several factors. The improved photocatalytic activities of 4.0-mol% and 6.0-mol% Pr-doped ZnO may result from the decrease of recombination rate of the photogenerated electron-hole pairs under the influence of the doped ions, which may capture the photogenerated electrons or holes in the photocatalytic process. Another reason is the narrowing of bandgap after doping. The photodegradation of rhodamine B is in accordance with the first-order kinetics at low concentration, which is based on the Langmuir–Hinshelwood model expressed as

$$-\ln(C/C_0) = kt, \tag{4}$$

where k is the reaction rate.[32] The kinetic rate of undoped ZnO is 3.220% min^{-1} and for 6.0-mol% Pr-doped ZnO, 5.490% min^{-1} [Fig. 9(b)], which exhibits that the photocatalytic property obtained from the best dopant quantity is enhanced by 1.7 times.

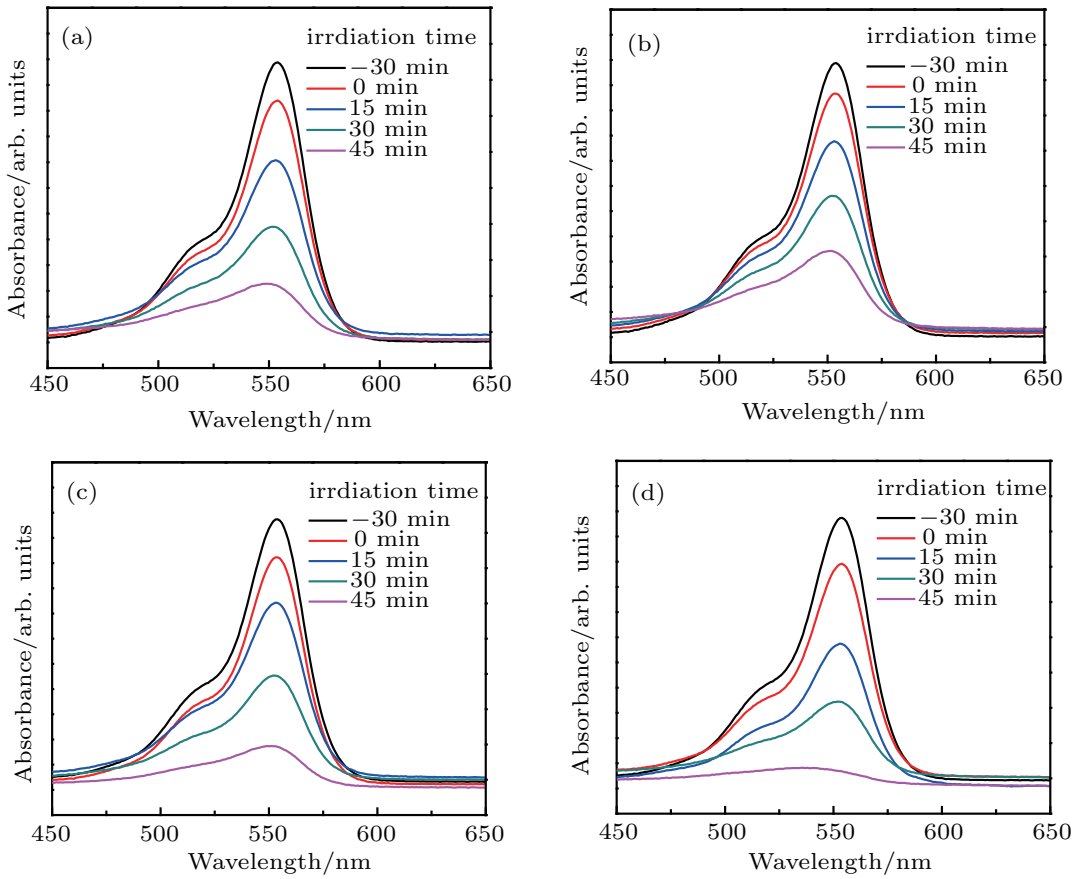


Fig. 7. (color online) UV-vis absorption spectra of the photodegradation of rhodamine B by (a) undoped, (b) 2-mol%, (c) 4-mol%, and (d) 6-mol% Pr-doped ZnO photocatalysts.

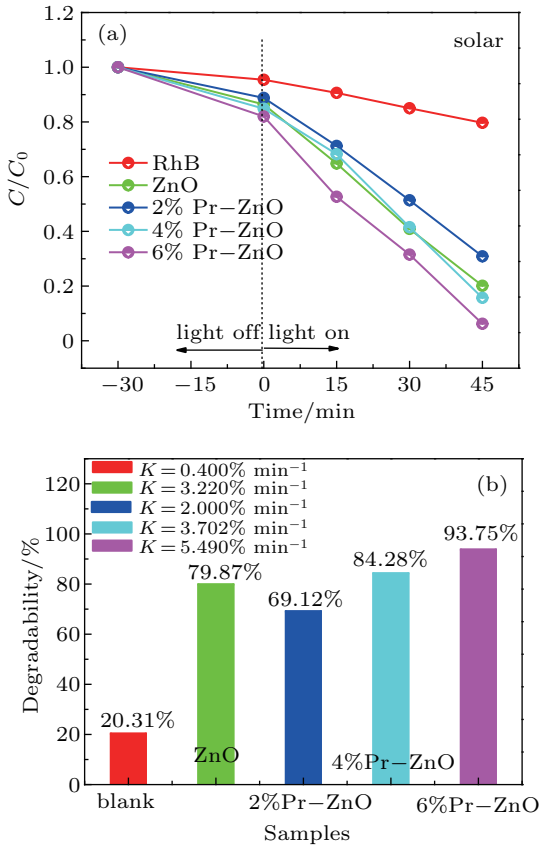


Fig. 8. (color online) (a) Photodegradation and (b) degradation rates of rhodamine B by using various photocatalysts irradiated with simulated sunlight for 45 min.

4. Conclusions

ZnO compounds with different doping concentration Pr (0 mol%–6.0 mol%) photocatalysts are prepared by the facile co-precipitating method. XRD and SEM analyses show that the photocatalysts are of hexagonal wurtzite phase and spherical morphology. XPS analysis shows the Zn–O and Pr–O bonding existing in the Pr-doped ZnO samples, which is supported by the FTIR measurement and reveals the chemical bonding and the presence of doping-related functional groups. The PL spectrum suggests the restraint of recombination rate of the photogenerated electrons and holes. UV-vis DRS shows that the bandgap for Pr-doped ZnO decreases slightly after Pr doping. The photocatalytic results show a 93.75%-degradation of rhodamine B by 6.0-mol% Pr-doped ZnO photocatalyst under the irradiation of simulated sunlight for 45 min.

References

[1] Sun J H, Dong S Y, Feng J L, Yin X J and Zhao X C 2011 *J. Mol. Catal. A: Chem.* **335** 145

[2] Khataee A, Karimi A, Arefi-Oskoui S, Darvishi Cheshmeh Soltani R, Hanifehpour Y, Soltani B and Joo S W 2015 *Ultrasonic Sonochem.* **22** 371

[3] Vaiano V, Matarangolo M, Sacco O, Sannino D 2017 *Appl. Catal. B* **209** 621

[4] Körbahti B K, Artut K, Geçgel C and Özer 2011 *Chem. Eng. J.* **173** 677

[5] Vaiano V, Matarangolo M, Sacco O and Sannino D 2017 *Chem. Eng. Trans.* **57** 625

[6] Ong C B, Ng L Y and Mohammad A W 2018 *Renewable Sustainable Energy Rev.* **81** 536

[7] Zhang J, Zhang Q X, Wang L H, Li X A and Huang W 2016 *Sci. Rep.* **6** 27241

[8] Zhang J, ChenA S, Wang L H, Li X A and Huang W 2016 *ACS Sus. Chem. & Eng.* **4** 4601

[9] Zhang J, Wang L H, Liu X H, Li X A and Huang W 2015 *J. Mater. Chem. A* **3** 535

[10] Zhang J, Wang Q, Wang L H, Li X A and Huang W 2015 *Nanoscale* **7** 10391

[11] Kant S, Pathania D, Singh P, Dhiman P and Kumar A 2014 *Appl. Catal. B* **147** 340

[12] Kant S, Kalia S and Kumar A 2013 *J. Alloys Compd.* **578** 249

[13] Hanifehpour Y, Soltani B, Amani-Ghadim A R, Hedayati B, Khomami B and Joo S W 2016 *J. Ind. Eng. Chem.* **34** 41

[14] Devi L G, Murthy B N and Kumar S G 2010 *Mater. Sci. Eng. B* **166** 1

[15] Manikandan A, Judith Vijaya J, John Kennedy L and Bououdina M 2013 *Ceram. Int.* **39** 5909

[16] Li D, Huang J, Cao L, Li J, Ouyang H and Yao C 2014 *Ceram. Int.* **40** 2647

[17] Divya N K and Pradyumnan P P 2017 *Bull. Mater. Sci.* **40** 1405

[18] Zhao Y, Fan B F, Chen Y T, Zhuo Y, Pang Z J, Liu Z and Wang G 2016 *Chin. Phys. B* **25** 078502

[19] Su Y Q, Chen M M, Su L X, Zhu Y and Tang Z K 2016 *Chin. Phys. B* **25** 066106

[20] Li D H, Wang H Q, Zhou H, Li Y P, Huang Z, Zheng J C, Wang J O, Qian H J, Ibrahim K, Chen X H, Zhan H H, Zhou Y H and Kang J Y 2016 *Chin. Phys. B* **25** 076105

[21] Hsu M and Chang C 2014 *J. Hazard. Mater.* **278** 444

[22] Vijayan T A, Chandramohan R, Valanarasu S, Thirumalai J and Subramanian S P 2008 *J. Mater. Sci.* **43** 1776

[23] Siriwong C, Wetchakun N, Inceesungvorn B, Channei D, Samerjai T and Phanichphant S 2012 *Prog. Cryst. Growth Charact. Mater.* **58** 145

[24] Uum Y R, Han B S, Lee H M, Hong S M, Kim G M and Rhee C K 2007 *Phys. Stat. Sol. (c)* **4** 4408

[25] Hamdy M S, Nickels P, Abd-Elmaksood I H, Zhou H, El-Mossalamy E H, Alyoubi A O, Lynch S, Nathan A and Thornton G 2012 *J. Photochem. Photobiol. A* **228** 1

[26] Ilanchezhiyan P, Kumar G M, Subramanian M and Jayavel R 2010 *Mater. Sci. Eng. B* **175** 238

[27] Thi V H and Lee B 2017 *Mater. Res. Bull.* **96** 171

[28] Vijayaprasath G, Murugan R, Hayakawa Y and Ravi G 2016 *J. Lumin.* **178** 375

[29] Geng B Y, Xie T, Peng X S, Lin Y, Yuan X Y, Meng G W and Zhang L D 2003 *Appl. Phys. A: Mater. Sci. Proc.* **77** 363

[30] Inoue Y, Okamoto M and Morimoto J 2006 *J. Mater. Res.* **21** 1476

[31] Yang W, Wang C, He J, Chang Y, Wang J, Chen L, Chen H and Gwo S 2008 *Phys. Stat. Sol. (a)* **205** 1190

[32] Tian Q Y, Wu W, Sun L L, Yang S L, Lei M, Zhou J, Liu Y, Xiao X H, Ren F, Jiang C Z and Roy V A L 2014 *ACS Appl. Mater. Interf.* **6** 13088